Title
NUMERICAL COMPUTATION OF BUOYANCY-INDUCED RECIRCULATION IN CURVED SQUARE DUCT LAMINAR FLOW

Authors
Chilukuri, R.
Humphrey, J.A.C.

Publication Date
1980-07-01

LBL-13274
Preprint

Lawrence Berkeley Laboratory
UNIVERSITY OF CALIFORNIA

Materials & Molecular Research Division

Published in the International Journal of Heat and Mass Transfer, Volume 24, 1981, pp. 305-314

NUMERICAL COMPUTATION OF BUOYANCY-INDUCED RECIRCULATION IN CURVED SQUARE DUCT LAMINAR FLOW

Radhakrishna Chilukuri and Joseph A.C. Humphrey

July 1980

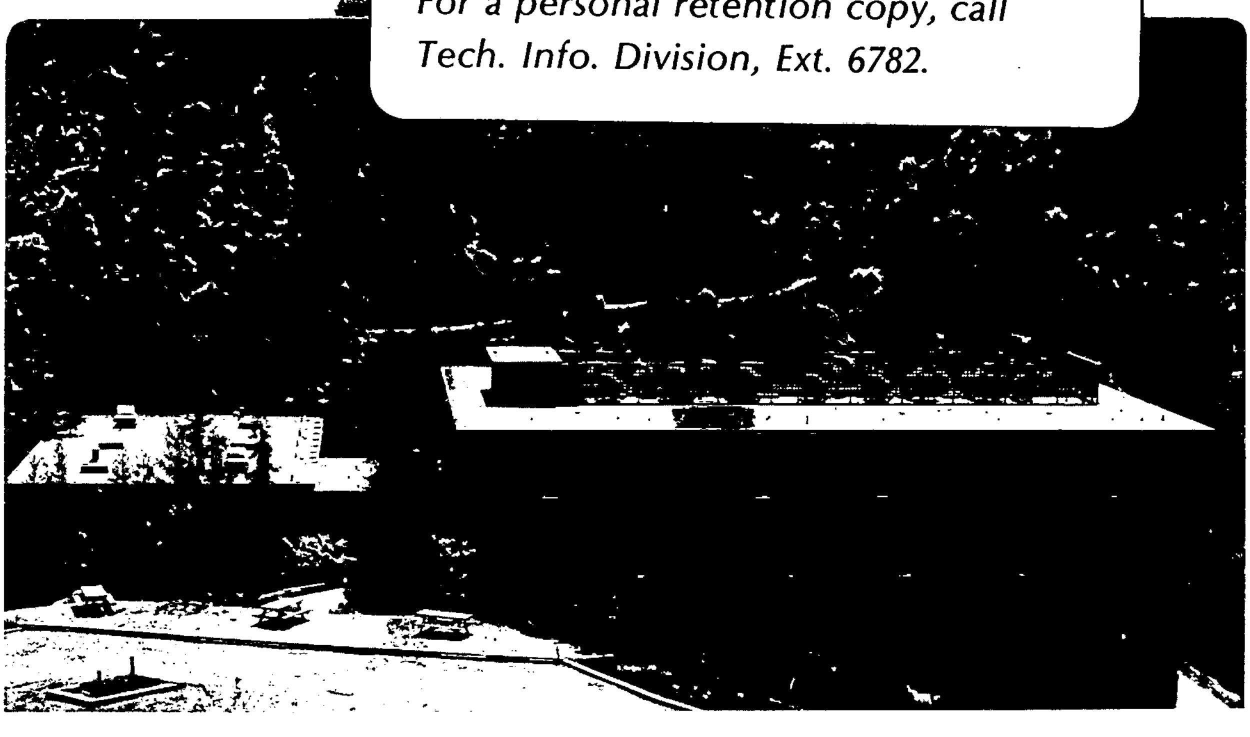

Prepared for the U.S. Department of Energy under Contract W-7405-ENG-48

DISCLAIMER

LBL-13274

NUMERICAL COMPUTATION OF BUOYANCY-INDUCED RECIRCULATION IN CURVED SQUARE DUCT LAMINAR FLOW

by

Radhakrishna Chilukuri
Research Graduate Student

and

Joseph A. C. Humphrey
Assistant Professor

Department of Mechanical Engineering
University of California, and the
Lawrence Berkeley Laboratory
University of California
Berkeley, CA 94720

July 1980

Revised Paper #IJ80/2185

This work was supported by the Division of Material Sciences, Office of Basic Energy Sciences of the U.S. Department of Energy under Contract number W-7405-ENG-48, and by a NSF Grant No. ENG 78-27007.

ABSTRACT

The influence of buoyant effects on developing heat transfer in strongly curved duct flows has been studied numerically for the special case of steady state, incompressible laminar flow of a constant physical property fluid to which the Boussinesq approximations apply. The two cases of: a) buoyant forces aligned with, and b) opposed to, the main flow direction were investigated. The presence of several streamwise recirculation zones necessitates the solution of fully elliptic transport equations. It is found that when buoyant forces are aligned with the main flow direction in curved duct flow geometries they can significantly enhance the rate of heat transfer, especially at the inner-radius wall. By contradistinction, when buoyant forces and the main flow are opposed, three additional elongated recirculation zones which appear at the inner-radius wall are the cause for reduced heat transfer to the flow in a curved duct.

NOMENCLATURE

c_p	specific heat capacity at constant pressure
De	Dean number ($\equiv$ Re $\sqrt{\frac{D_H/2}{Rc}}$)
D_H	hydraulic diameter
g	gravitational constant
Gr	$\rho^2 g\beta(T_w - T_{in})D_H{}^3/\mu^2$
k	thermal conductivity
n	coordinate normal to duct wall
Nu	local Nusselt number
$\overline{Nu}$	perimeter averaged Nu
P	pressure
Pr	Prandtl number ($\equiv \frac{\mu c_p}{k}$)
q	heat flux
r	radial coordinate
r_i	inner-radius wall of curved duct
r_o	outer-radius wall of curved duct
R_c	mean radius of curvature
Re	Reynolds number ($\equiv D_H\rho V_B/\mu$)
T	temperature
T_B	bulk temperature
T_{in}	inlet flow temperature
T_w	wall temperature
v_r	radial velocity component
v_z	axial (spanwise) velocity component
v_ϕ	longitudinal (streamwise) velocity component
V_B	bulk average velocity
x_p	coordinate along duct periphery; $x_p = 0$ corresponds to $r = r_i$ on symmetry plane

z	axial (spanwise) coordinate
β	coefficient of thermal expansion
μ	viscosity
ρ	density
ϕ	longitudinal coordinate (streamwise direction)

INTRODUCTION

While numerical calculation schemes will probably never substitute entirely the experimental investigation of engineering flows, they have already proven extremely useful for exploring and helping to optimize fairly complicated flow systems in which measurements are difficult, costly or laborious to obtain. Developing flows in curved ducts are in this class of flows. In this case, three-dimensionality and, at high velocity, turbulence effects impart a high degree of complexity to the flow.

Although curved duct flows have and continue to be investigated experimentally, a substantial portion of the knowledge acquired derives from analytical studies and, more recently, detailed numerical calculations. A review of experimental, analytical and numerical studies up to 1975 is given in [1]. Examples of analytical and numerical studies for the laminar flow regime are given in [2-6], and for the turbulent flow regime (using two-equation turbulence models) in [7-9]. While the laminar flow cases have yielded to numerical prediction and are currently limited mainly by cost considerations dictated by computational time and storage requirements, calculations of corresponding turbulent flows are less accurate [9].

Motions driven by buoyant forces arise in flows in which $Gr/Re^2 \gtrsim 1$. In ducts with curvature the criterion is given by $Gr/De^2 \gtrsim 1$, where the Dean number (De) characterizes the intensity of the cross-stream flow driven by an imbalance between centrifugal and radial pressure-gradient induced forces. Depending on the relative orientation (with respect to gravity) of a curved duct geometry and the ratio of buoyant to inertial forces, reversed flow regions can be expected to appear in curved duct flows subjected to thermal effects. Examination of the literature published to date suggests that, although forced convection heat transfer has been investigated (see, for example, [5]), thermally induced buoyant motion in developing curved duct flow has received comparatively little attention [2,10,11]. This is the case in spite of the relative ease with which conditions are attained propitious to the occurrence of the phenomenon. Thus, the attendant consequences on heat and mass transfer remain unknown for many systems of practical interest with natural convection present. Such systems include coiled chemical reactors, bends and tees in gas and oil pipelines, ventilating conduits in buildings, and various types of clinical flows. For example, in a coiled tube with a chemical (or chemical reaction) sensitive to localized temperature differences, it would be desirable to know the number and extent of regions of flow reversal induced by buoyant motion as well as the intensity of the latter.

The lack of detailed experimental information bearing on buoyant motions in curved passages with heat transfer is probably due, in part, to serious difficulties and large uncertainties associated with measurement techniques in such flows. While some of the difficulties and experimental uncertainty can be removed by using non-intrusive techniques, such as laser-Doppler velocimetry for measurements of velocity, the insertion of probes for measuring temperature will perturb the flow. Perturbations of this nature would be especially severe in regions of flow reversal. Given the considerable difficulties associated with making measurements, it is surprising to find that no attempt has been made (to the authors' knowledge) to investigate numerically the influence of buoyant effects on the motion and heat transfer in developing curved duct flows. In principle, the accuracy of such computations in the laminar flow regime for an incompressible fluid are limited only by the nature of the equations solved (parabolic, semi-elliptic or elliptic)[1] and the error incurred

[1]For flows in ducts of mild curvature wherein longitudinal and cross-stream pressure variation can be decoupled, calculation schemes based on parabolic forms of transport equations [6] (boundary layer equations) may be used. For stronger curvature it is necessary to account more exactly for ellipticity in the pressure field [12], or resort to semi-elliptic or fully elliptic calculation schemes which allow for the direct determination of pressure [3-5, 8, 9].

through numerical diffusion. Notwithstanding these limitations, provided that the integrity of the physics is maintained in the relevant transport equations and boundary conditions, computations of sufficient accuracy for engineering purposes can be made [5].

The present numerical study was motivated by the need to learn the extent and magnitude of thermally induced buoyant motions, and their tendency to produce recirculation, in ducts of strong curvature. Attention was focused on the laminar flow regime principally because of the uncertainties (and expense) associated with presently available models for the turbulent flow regime. However, except for systems with unusually high energy fluxes, the relative influence of buoyant forces would be expected to decrease with increasing Re. Due to the expensive nature of the calculations, these were limited to a geometry of square cross-section and of radius ratio $R_c/D_H = 2.3$ in the curved section. It is presumed that the calculated results are representative of a range of flows with not too dissimilar dynamic, thermal and geometrical characteristics.

CASE STUDIES AND FLOW CONDITIONS

Two sets of calculations were made for the geometry shown in Figure 1. In both cases the 90 degree curved section and exit tangent were vertically aligned, with the entrance tangent always in the horizontal plane. In one case (A), however, the exit tangent flow was aligned with the direction of gravity, while in the other (B) it was opposed to the direction of gravity. In both cases all the walls in the curved section were fixed at a temperature T_W higher than the entrance flow, with adiabatic conditions imposed at all the remaining walls in the connecting tangent sections. The entrance and exit tangents were 5.8 and 12 hydraulic diameters long, respectively, and ensured that the flow in the curved section was sufficiently removed from the boundary conditions imposed at the entrance plane in the upstream tangent and the exit plane in the downstream tangent. The dimensionless parameters characterizing the flows were: $Re = 787$, $De = 367$, $R_C/D_H = 2.3$, $|Gr| = 3.14 \times 10^5$ and $Pr = 1.0$. The choice of conditions was dictated by the availability in [3] of corresponding measurements and calculations of this flow in the absence of thermal effects.

EQUATIONS, BOUNDARY CONDITIONS AND CALCULATION PROCEDURE

Calculations were based on fully elliptic, three-dimensional finite difference forms of the steady state conservation equations for momentum and energy. The calculation scheme and its testing have already been described in detail in [3,4]. Its extension and validation for predicting forced convection heat transfer in curved duct flows may be found in [5]. A brief outline is given here of the adaptation of the calculation scheme in [5] to flows with buoyant effects to which the Boussinesq approximation apply.

Equations

Transport equations in cylindrical coordinates[2] for a steady, incompressible, variable temperature, laminar flow are given by:

Continuity.

$$\frac{\partial v_r}{\partial r} + \frac{1}{r}\frac{\partial v_\phi}{\partial \phi} + \frac{\partial v_z}{\partial z} + \frac{v_r}{r} = 0 . \qquad (1)$$

Momentum.

$$\rho\left[v_r \frac{\partial v_r}{\partial r} + \frac{v_\phi}{r}\frac{\partial v_r}{\partial \phi} + v_z \frac{\partial v_r}{\partial z} - \frac{v_\phi{}^2}{r}\right] = -\frac{\partial P}{\partial r}$$

$$+ \mu\left[\nabla^2 v_r - \frac{v_r}{r^2} - \frac{2}{r^2}\frac{\partial v_\phi}{\partial \phi}\right]$$

$$- \left[-g \cos \phi + \frac{v_\phi{}^2}{r}\right]\rho\beta(T - T_{in}) \qquad (2)$$

[2]In the upstream and downstream tangents, calculations were performed using equations expressed in terms of rectangular coordinate notation. Boundary conditions were overlapped between duct sections as explained in [3].

$$\rho\left[v_r\frac{\partial v_\phi}{\partial r}+\frac{v_\phi}{r}\frac{\partial v_\phi}{\partial \phi}+v_z\frac{\partial v_\phi}{\partial z}+\frac{v_r v_\phi}{r}\right]=-\frac{1}{r}\frac{\partial P}{\partial \phi}$$

$$+\mu\left[\nabla^2 v_\phi+\frac{2}{r^2}\frac{\partial v_r}{\partial \phi}-\frac{v_\phi}{r^2}\right]$$

$$+\left[-g\sin\phi+\frac{v_r v_\phi}{r}\right]\rho\beta(T-T_{in}) \qquad (3)$$

$$\rho\left[v_r\frac{\partial v_z}{\partial r}+\frac{v_\phi}{r}\frac{\partial v_z}{\partial \phi}+v_z\frac{\partial v_z}{\partial z}\right]=-\frac{\partial P}{\partial z}+\mu\nabla^2 v_z \qquad (4)$$

Energy.

$$\rho\, c_p\left[v_r\frac{\partial T}{\partial r}+\frac{v_\phi}{r}\frac{\partial T}{\partial \phi}+v_z\frac{\partial T}{\partial z}\right]=k\left[\nabla^2 T\right] \qquad (5)$$

where

$$\nabla^2=\frac{\partial^2}{\partial r^2}+\frac{1}{r}\frac{\partial}{\partial r}+\frac{1}{r^2}\frac{\partial^2}{\partial \phi^2}+\frac{\partial^2}{\partial z^2} \qquad (6)$$

These equations correspond to the buoyancy-opposed flow geometry in Figure 1. For a buoyancy-assisted flow geometry, the sign for g in the momentum component equations must be reversed.

The Boussinesq approximations [13,14] have been used in deriving the forms of the equations given above. The range of validity of the approximate equations has been documented in [14] for the case of natural convection in a horizontal fluid layer, corresponding to the Rayleigh-Bernard problem.

Boundary Conditions

It is required to solve (1)-(5) together with the boundary conditions given below.

Entrance plane (upstream tangent).

$$v_r = v_z = 0,\ v_\phi = \text{developed duct flow} \tag{7}$$

$$T = T_{in}$$

Exit plane (downstream tangent).

$$\frac{\partial v_r}{\partial \phi} = \frac{\partial v_z}{\partial \phi} = \frac{\partial v_\phi}{\partial \phi} = \frac{\partial T}{\partial \phi} = 0 \tag{8}$$

with overall continuity of mass and energy imposed.

Side walls.

$$v_r = v_z = v_\phi = 0 \tag{9}$$

$T = T_w$ at all walls in the curved duct

$q = 0$ at all walls in upstream and downstream tangents.

Symmetry plane.

$$v_z = \frac{\partial v_r}{\partial z} = \frac{\partial v_\phi}{\partial z} = \frac{\partial T}{\partial z} = 0 \tag{10}$$

Calculation Procedure

Finite difference equations are obtained by integrating (1)-(5) over volume elements or "cells" discretizing the flow domain. The velocity components, pressure and temperature are the dependent variables computed on a number of staggered, interconnected grids, each of which is associated with a specific variable. The general form of the finite difference expression is given by

$$\phi_P = \left(\sum_{i=1}^{6} A_i \phi_i + S_o\right) \Bigg/ \left(\sum_{i=1}^{6} A_i + S_P\right) \tag{11}$$

where ϕ_P (velocity component, pressure or temperature) is the variable solved for at a position P in the discretized flow domain. The A_i coefficients are determined at the cell surfaces and represent the combined contributions of convection and diffusion to the balance of ϕ. Other contributions arising from temperature pressure, centrifugal and gravitational forces (sources or sinks) are contained in S_o while the effects of the Coriolis force are contained in S_P. Detailed forms for S_o and S_P in variable property flows are available in [15].

Solution of the system of finite difference transport equations with appropriately differenced boundary conditions is achieved by means of a cyclic series of predictor-corrector operations as described in [3,4]. Briefly, the method involves using an initial or intermediate value of the pressure field to solve for an intermediate velocity field. A pressure correction to the pressure field is determined by bringing intermediate velocities into conformity with continuity. Corrections to the pressure and velocity fields are applied and the energy equation is solved for T (in flows where energy and momentum are not linked through temperature effects this last step can be taken after the velocity and pressure fields have been determined). The above steps are repeated until some pre-established convergence criterion is satisfied.

It has been shown in [3-5] that fully elliptic, three-dimensional computations of sufficient accuracy for engineering purposes can be obtained on fairly coarse, unequally spaced grids. Because of cost considerations, no attempt was made here to produce grid-independent results. Calculations were performed on an unequally spaced grid covering a symmetrical half of the ducted flow. The grid had 15 nodes in the radial direction, 12 in the axial and 50 in the streamwise (longitudinal) direction. The streamwise nodes were unequally distributed with 12 nodes in the upstream tangent and 19 nodes in the curved and downstream sections, respectively. Typical computation times and storage requirements for converged solutions were 1870 CPU seconds and 171 K_8 words on a CDC 7600 machine. Strong radial variations in longitudinal pressure gradient and the presence of streamwise recirculation precluded the use of numerically more exact (and relatively inexpensive) parabolic or semi-elliptic calculation schemes.

For the value of Gr studied here, noteworthy difficulties related to stability or convergence due to the presence of buoyant effects were not encountered. However, depending on the calculation case, under-relaxation factors for both pressure and velocities were varied from 0.1 to 0.75. Relative to a non-buoyant reference flow, the buoyant cases took about 1.3 times longer to attain a converged solution. It should be noticed that the relative contributions of the body forces to momentum balance in the curved duct section varied with angular position. For the flow conditions studied, maximum values of the centrifugal and Coriolis body forces $((v_\phi{}^2/r)\ \rho\beta(T - T_{in})$ and $(v_r v_\phi/r)\ \rho\beta(T - T_{in})$ respectively) were always less than 0.1% of the corresponding gravity terms and, hence, negligibly small. Nevertheless, the influence of centrifugal and Coriolis forces could be significant in a gravitational-free situation and, therefore, were retained in the present formulation.

At high values of Grashof ($Gr \simeq 3 \times 10^6$), serious convergence problems were encountered. The instability was not in the nature of that described in, for example, [16], due to large Coriolis forces. More likely it was related to the pressure correction technique derived by substitution of linearized velocity expression (in terms of pressure) into the continuity equation [17]. The behavior at high Gr was exactly similar to not using sufficiently low under-relaxation factors when calculating the reference and low Gr number cases. Further lowering of the under-relaxation factors would have led to unrealistically long calculation times for converged solutions at high Gr. To avoid this approach, other possible remedies were investigated such as to:

a) Impose lower values for under-relaxation of the buoyancy terms during the early cycles of calculation and increase these slowly; b) Commence buoyant calculation cases from the converged solution for the reference case and then "turn on" buoyant effects; c) Evaluate conduction effects before attempting to calculate velocities in order to reduce the initial steep variations of temperature at heated walls; d) Use combinations of the above. None of these approaches was effective in helping to remove the instability.

Finally, it should be mentioned that the presence of streamwise recirculation in the downstream tangent required that this section be long enough in order to set $\partial/\partial\phi = 0$ boundary condition at the exit plane. The influence of this condition was very small on the downstream tangent flow and completely negligible for the flow in the curved duct section.

DISCUSSION OF CALCULATED RESULTS

Calculations were performed for the two cases described above and for a reference flow of identical conditions [5] in which buoyant contributions to heat transfer were neglected. In all cases, regions of streamwise flow reversal were predicted.

Two recirculation zones, common to the three cases, were found to occur in the curved duct section and were symmetrically located at the outer-radius wall corners. Thus, for example, Figure 2 shows, in the form of equal value dimensionless v_ϕ contours the size and location of one of the symmetrical recirculation zones for the case of ϕ = 16.87 degrees in the buoyancy-opposed flow geometry. For the cases of buoyancy-opposed flow and the non-buoyant reference flow, these two recirculation zones extended from approximately $\phi = 0$ to $\phi = 34$ degrees. The same recirculation zones were about half as large, extending from $\phi = 11$ to $\phi = 23$ degrees, and were less intense in the case of the buoyancy-assisted flow. The maximum reverse flow velocities in these zones, for each case, were as follows: $v_\phi/V_B \lesssim 0.17$ for buoyancy-opposed flow; $v_\phi/V_B \lesssim 0.06$ for buoyancy-assisted flow; $v_\phi/V_B \lesssim 0.11$ for the reference non-buoyant flow. Similar regions of flow reversal have been predicted and discussed in [3-4]. The phenomenon is due to an unfavorable longitudinal pressure gradient near the outer-radius wall at the entrance to the curved duct. However, present results show that when buoyant effects oppose the main flow (Case A), flow recirculation is intensified. By contradistinction, when buoyant effects are aligned with the main flow (Case B), both the size and intensity of the recirculation zones are substantially reduced.

In addition to the outer-corner reversed flow regions, the buoyancy-opposed flow showed three more zones of flow reversal at the inner radius wall. These may be seen in Figure 3, corresponding to a longitudinal position of ϕ = 61.87

degrees. The single recirculation zone located on the symmetry plane extended from ϕ = 34 degrees in the curved duct to a distance 1.33 hydraulic diameters into the downstream tangent. The smaller symmetrical reversed flow zones in the corners extended from about ϕ = 34 degrees to 0.25 hydraulic diameters into the downstream tangent. The maximum reversed flow on the symmetry plane was v_ϕ/V_b = 0.18 at ϕ = 61 degrees, and v_ϕ/V_B = 0.05 at the corners for ϕ = 45 degrees.

Non-dimensional profiles of the main flow velocity component (v_ϕ/V_B) and temperature $(T_w - T)/(T_w - T_{in})$ are given in Figures 4 and 5 for various longitudinal stations located on the duct symmetry plane. At about ϕ = 45 degrees, significant differences already appear among the velocity profiles with the differences becoming especially accentuated at the further downstream stations. Relative to the reference case, in the flow where buoyant forces oppose the main flow direction (Case A), the results show the main flow accelerating near the outer-radius wall while decelerating near the inner-radius wall. By contrast, in the flow where buoyant forces reinforce the main flow (Case B), the calculations show the main flow component decelerating near the outer-radius wall while accelerating near the inner-radius wall. Thus in the buoyancy-assisted flow case, the net effect of buoyancy is to distribute more evenly the longitudinal component of momentum. This last remark is partly supported by the transverse velocity component profiles (v_r/V_B and v_z/V_B) shown in Figure 6 at a longitudinal station of ϕ = 47.8 degrees, and the vector plots for transverse components at 87 degrees, shown in Figures 7 and 8. The relatively large levels of v_z/V_B in the vicinity of the inner-radius wall for the case of buoyancy-assisted flow are further indications of the evening out effect being produced by buoyant forces on the longitudinal component of momentum. By comparison, corresponding values of v_z/V_B at the same locations for buoyancy-opposed flow are weak, even though large values of v_r/V_B and v_z/V_B arise near the outer-radius wall.

The temperature profiles given in Figure 5 do not show the marked differences of the longitudinal velocity component. Nevertheless, the differences which do arise are in basic agreement with the discussion presented above in connection with the velocity components as influenced by buoyant effects. It is worth noting that, in passing from the bend into the downstream tangent, the buoyancy-assisted flow attains a higher average temperature than the buoyancy-opposed flow.

The peripheral variation of local Nusselt number (calculated from Nu = $(\partial T/\partial n \times D_H)/(T_w - T_B)$ is shown in Figure 9 at a location of $\phi = 87$ degrees in the curved duct section. Values for Nu have been set to 0 at the duct corners. The largest differences between Nu arise at the inner-radius wall. It is clear that the net result of buoyancy at this wall is to enhance heat transfer to the flow, by a factor of about 2, when buoyant forces are aligned with (rather than opposed to) the main flow direction. Reduced heat transfer at the inner-radius wall in the case of the buoyancy-opposed flow is due to the appearance there of three regions of flow reversal; see Figures 3 and 7 where the latter figure shows substantially reduced secondary motion near the inner radius wall.

Longitudinal variations of mean Nusselt number as a function of longitudinal position in the curved duct are given in Figure 10. In general, higher rates of heat transfer always arise for the case of buoyant forces aligned with the main flow. The slightly smaller initial values of $\overline{Nu}$ for the buoyancy-opposed flow (relative to the non-buoyant reference case) are related to the symmetrical flow reversals at the outer-radius wall. At larger ϕ, the $\overline{Nu}$ for this case increases and overtakes corresponding values for the reference case. This is partly explained by noting that inner-wall recirculation zones for this case constrict the main flow and force steeper gradients of v_ϕ at the outer-radius wall, thus increasing the overall transfer of heat to the flow.

CONCLUSIONS

A numerical study has been conducted to determine the relative influence of buoyant effects in developing curved duct flows to which the Boussinesq approximation apply. It is believed that these computations are the first of their kind. Although limited by cost considerations to a specific geometry and flow conditions, the results are of value for helping to understand the role played by buoyant forces in enhancing or diminishing heat transfer to flows in ducts with strong curvature.

In the vertically aligned geometries considered here, recirculation zones were predicted at the outer-radius wall for all cases, and at the inner-radius wall also for the case of buoyant forces opposed to the main flow direction. Maximum values of reversed flow intensity were given by $v_\phi/V_B \lesssim 0.17 - 0.18$ at the outer-and inner-radius walls of the flow geometry for the case of buoyant forces and main flow direction opposed.

When buoyant forces are aligned with the main flow, their effect is to enhance heat transfer to the flow and to even out the cross-stream plane distribution of streamwise momentum. This effect is particularly noticeable at the inner-radius wall, where local values of the Nusselt number can increase two-fold relative to corresponding values in a buoyancy-opposed flow geometry.

The existence of strong radial variations in longitudinal pressure gradients and of reversed flow regions has imposed the need to deal with fully elliptic transport equations. Unfortunately, these are expensive to solve in terms of calculation times and storage requirements. However, because it has been shown in earlier studies that realistic calculations can be performed on unequally spaced grids of the refinement used in this study, these and similar results should be of use for engineering purposes.

ACKNOWLEDGEMENTS

The present study was made possible through NSF Grant No. ENG 78-27007. Partial financial support for the numerical computations was provided by the Division of Material Sciences, Office of Basic Energy Sciences, U.S. Department of Energy under contract number W-7405-ENG-48. Thanks are due to Mr. G. Yee for his assistance in the early stages of this work. We are grateful to Mrs. Carol Chiang for preparation of the manuscript. Part of this work was the topic for a paper presented at the ASME Winter Annual Meeting in Chicago, Nov. 1980.

REFERENCES

1. Humphrey, J.A.C., "Flow in Ducts with Curvature and Roughness," Ph.D. Thesis, University of London, 1977.

2. Yao, L-S and Berger, S. A., "Flow in Heated Curved Pipes," Journal of Fluid Mechanics, 88, 1978, p. 339.

3. Humphrey, J.A.C., Taylor, A.M.K. and Whitelaw, J. H., "Laminar Flow in a Square Duct of Strong Curvature," Journal of Fluid Mechanics, Vol. 83, Part 3, 1977, pp. 509-527.

4. Humphrey, J.A.C., "Numerical Calculation of Developing Laminar Flow in Pipes of Arbitrary Curvature Radius," Canadian Journal of Chemical Engineering, Vol. 56, 1978, pp. 151-164.

5. Yee, G., Chilukuri, R. and Humphrey, J.A.C., "Developing Flow and Heat Transfer in Strongly Curved Ducts of Rectangular Cross-Section," Journal of Heat Transfer, Vol. 102, 1980, pp. 285-291.

6. Ghia, K. N. and Sokhey, J. S., "Laminar Incompressible Viscous Flow in Curved Ducts of Rectangular Cross-Sections," Journal of Fluids Engineering, Transactions of the ASME, Vol. 99, 1977, pp. 640-648.

7. Patankar, S. V., Pratap, V. S. and Spalding, D. B., "Prediction of Turbulent Flow in Curved Pipes," Journal of Fluid Mechanics, Vol. 67, 1975, p. 583.

8. Pratap, V. S. and Spalding, D. B., "Numerical Computation of the Flow in Curved Ducts," Aeronautical Quarterly, Vol. 26, 1975, p. 219.

9. Humphrey, J.A.C., Whitelaw, J. H. and Yee, G., "Turbulent Flow in a Square Duct with Strong Curvature," University of California, LBL, Report No. 9650, 1979.

10. Akiyama, M., Suzuki, Ma., Suzuki, Mi., and Nishimaki, I., "Mixed Convection Problems in the Entrance Region of Curved Circular Tubes," Procs. 17th Japan Heat Transfer Symposium, 1980.

11. Moshfegian, M. and Bell, K. J., "Local Heat Transfer Measurements in and Downstream from a U-Bend," ASME Paper No. 79-Ht-82.

12. Moore, J. and Moore, J. G., "A Calculation Procedure for Three-Dimensional, Viscous, Compressible Duct Flow. Part I - Inviscid Flow Considerations," Paper No. 79-WA/FE-4, ASME Winter Annual Meeting, December 2-7, 1979, New York.

13. Speigel, E. A. and Veronis, G., "On the Boussinesq Approximation for a Compressible Fluid," Astrophysics Journal, Vol. 131, 1960, pp. 442-447.

14. Gray, D. D. and Giorgini, A., "The Validity of the Boussinesq Approximation for Liquids and Gases," International Journal of Heat and Mass Transfer, Vol. 19, 1976, pp. 545-551.

15. Humphrey, J.A.C., "Numerical Calculation of Variable Property Flows in Curvilinear Orthogonal Coordinates," Canadian Journal of Chemical Engineering, Vol. 56, 1978, pp. 624-626.

16. Pollard, A. and Thyagaraja, A., "A New Method for Handling Flow Problems with Body Forces," Computer Methods in Applied Mechanics and Engineering, Vol. 19, 1979, pp. 107-116.

17. Patankar, S. V., "Numerical Prediction of Three-Dimensional Flows," in Studies in Convection, Vol. 1, edited by B. E. Launder, Academic Press, London, 1975, pp. 1-79.

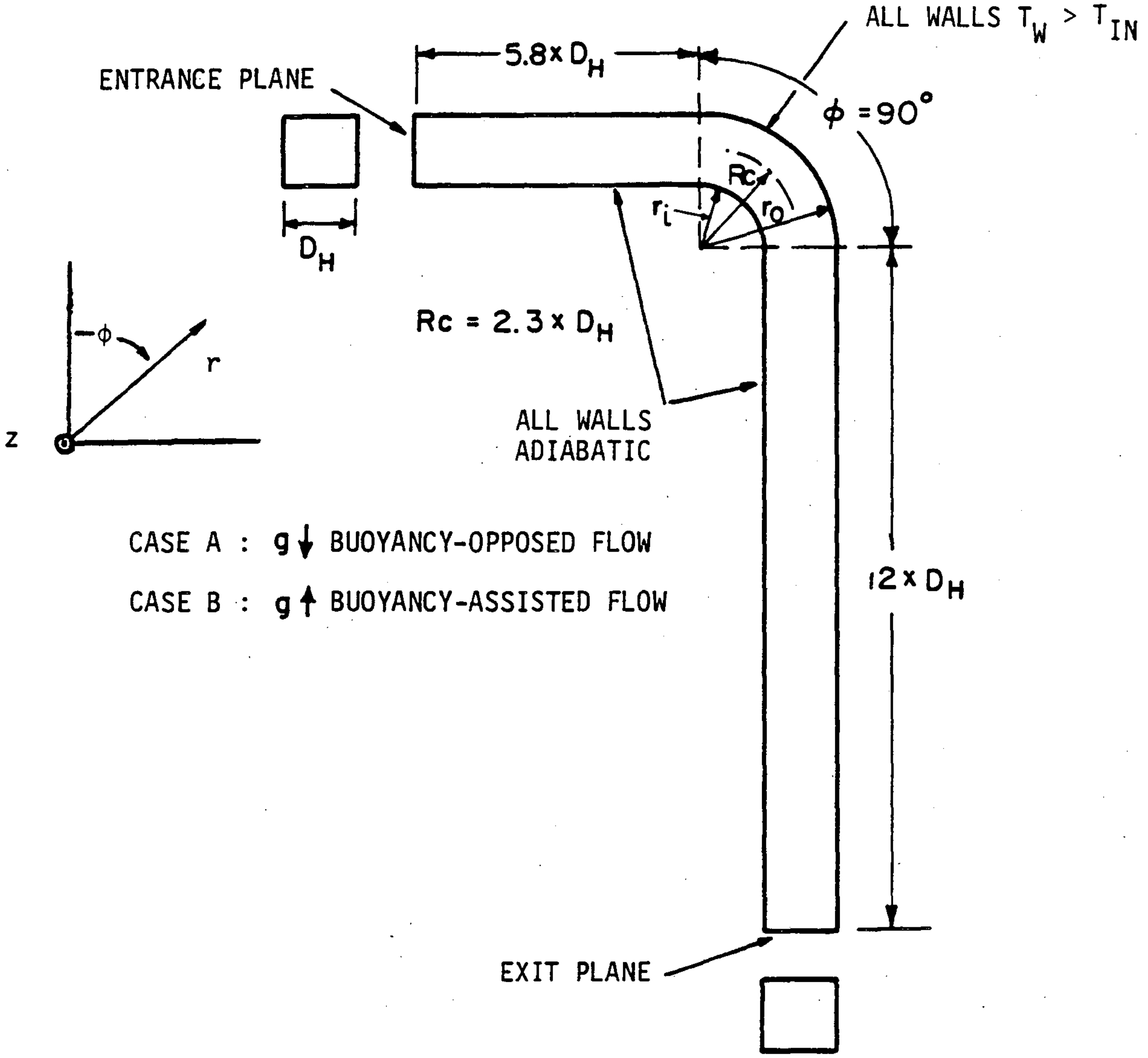

XBL 819-1902

Figure 1 Coordinate system and calculated curved duct geometry indicating relative orientation of gravity. Case A, buoyancy-opposed flow; Case B, buoyancy-assisted flow.

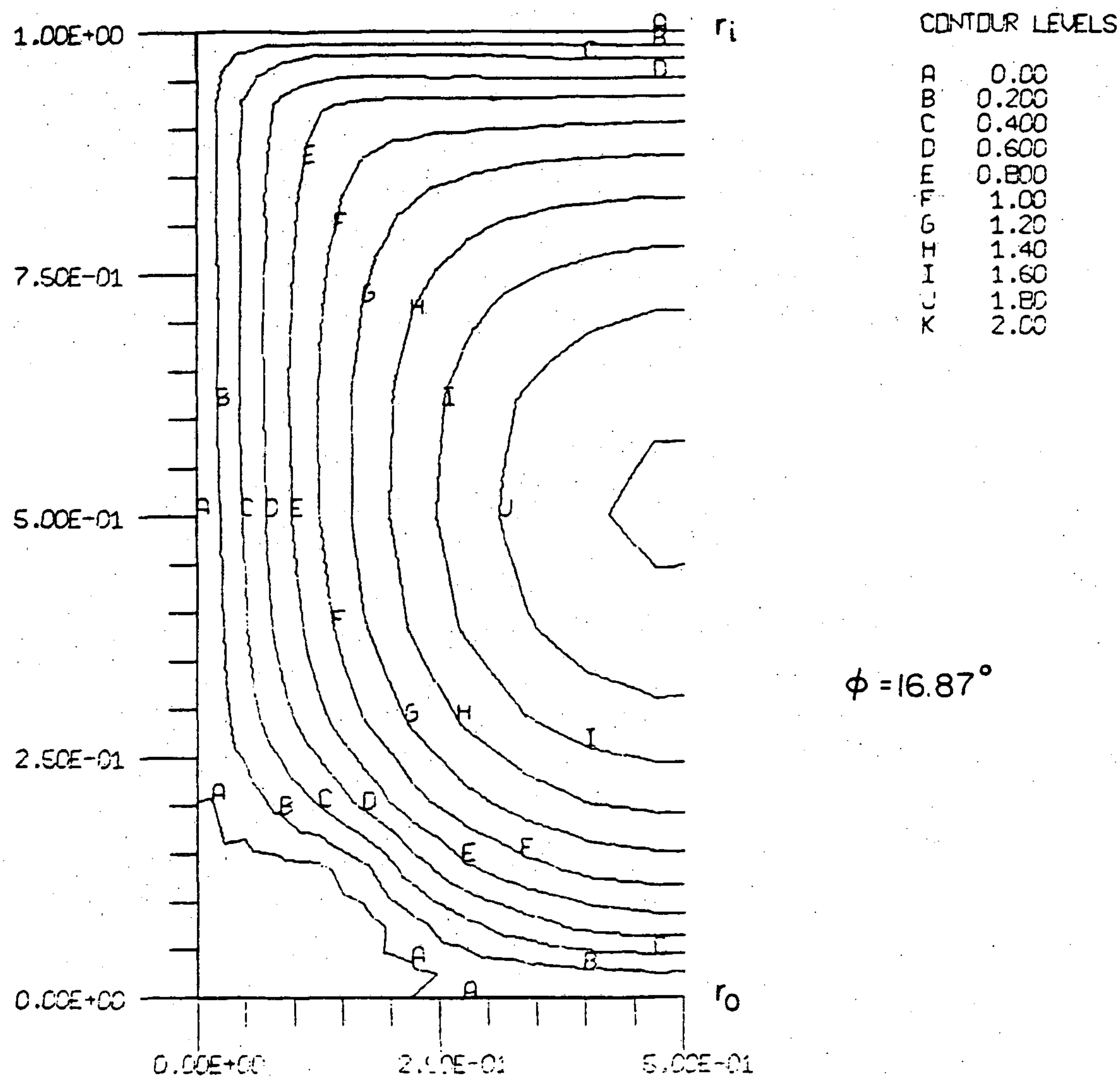

XBL 819-1900

Figure 2 Isovelocity contours of v_ϕ/V_B at ϕ = 16.87 degrees in the curved duct section; case of buoyancy-opposed flow. Recirculation zone bounded by contour level A and walls.

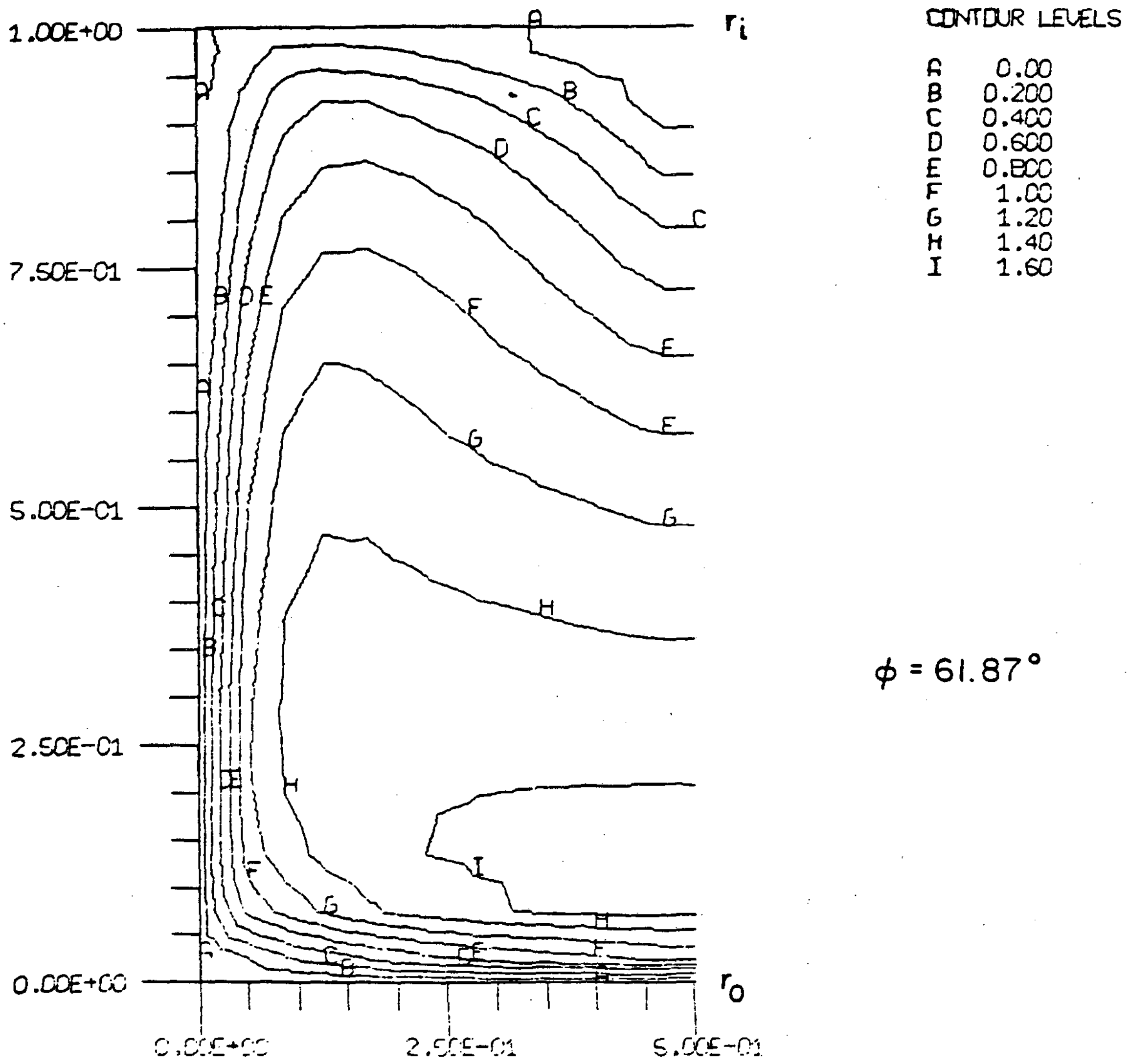

XBL 819-1908

Figure 3 Isovelocity contours of v_ϕ/V_B at ϕ = 61.87 degrees in the curved duct section; case of buoyancy-opposed flow. Recirculation zones bounded by contour levels A and walls.

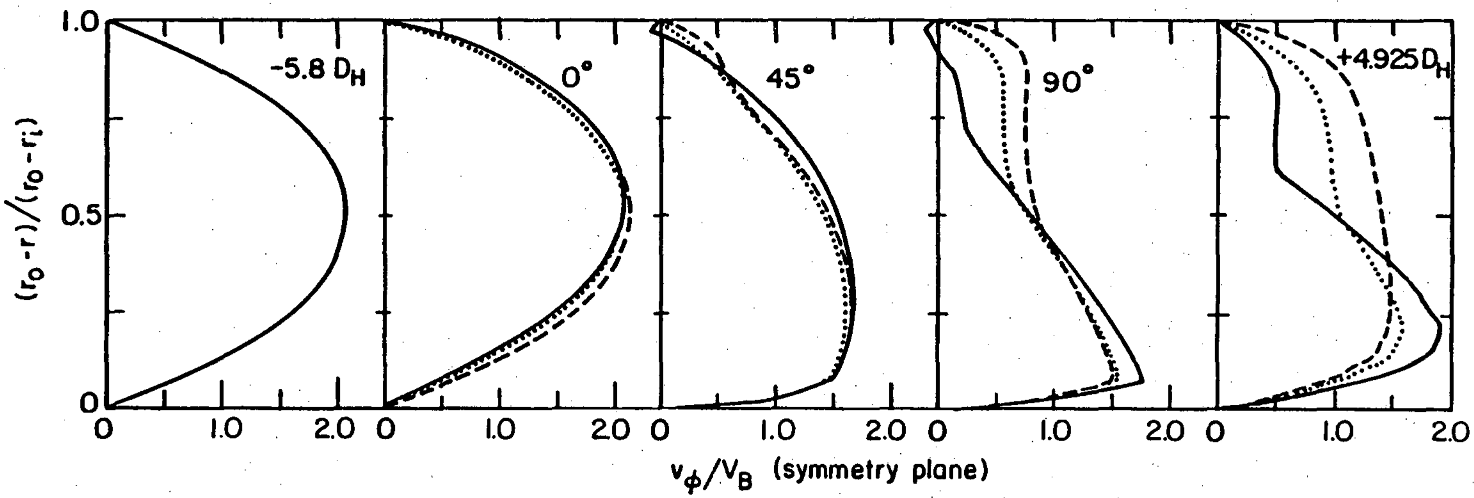

XBL 819-1907

Figure 4 Radial variation of v_ϕ/V_B as a function of longitudinal position. Profiles are located on the duct symmetry plane: (...) non-buoyant flow, (---) buoyancy-assisted flow (-) buoyancy-opposed flow.

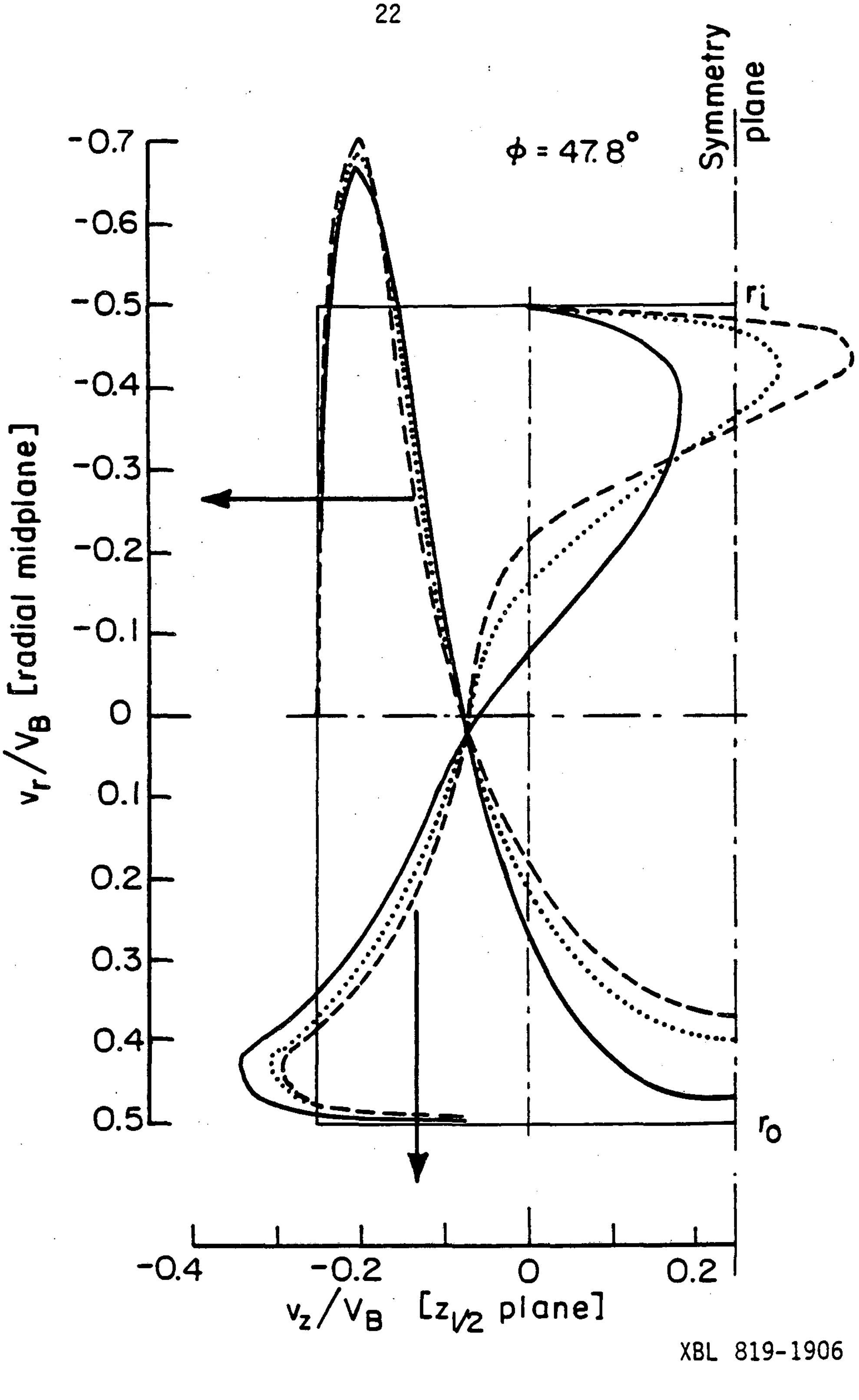

Figure 5 Radial and axial variation of transverse velocity components v_r/V_B and v_z/V_B at ϕ = 47.8 degrees in the curved duct section: (...) non-buoyant flow, (---) buoyancy-assisted flow, (-) buoyancy-opposed flow.

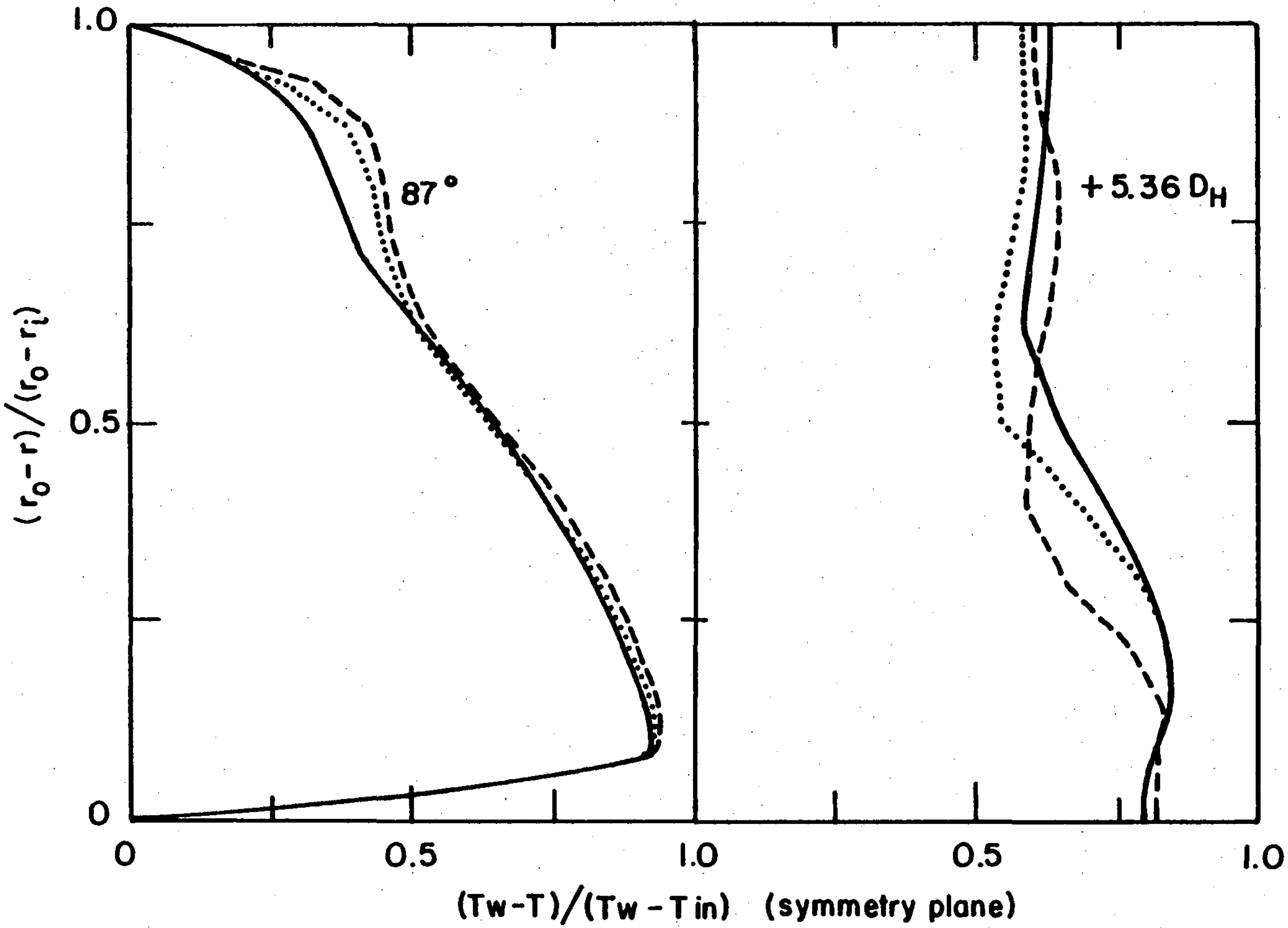

XBL 819-1905

Figure 6 Radial variation of temperature at two longitudinal positions. Profiles are located on the duct symmetry plane: (...) non-buoyant flow, (---) buoyancy-assisted flow, (-) buoyancy-opposed flow.

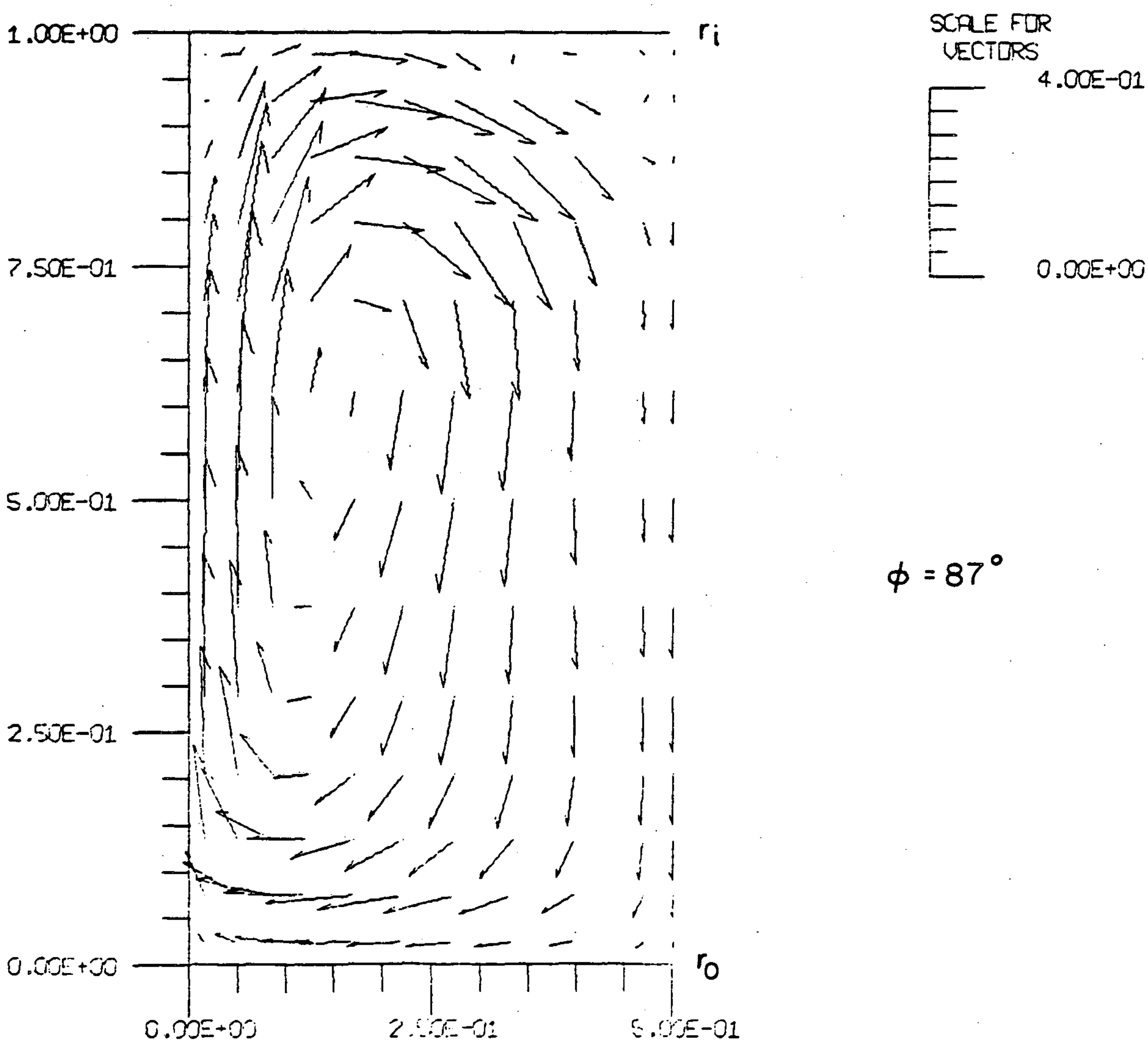

XBL 819-1904

Figure 7 Vector plot of cross-stream velocity components at ϕ = 87 degre in the curved duct section; case of buoyancy-opposed flow.

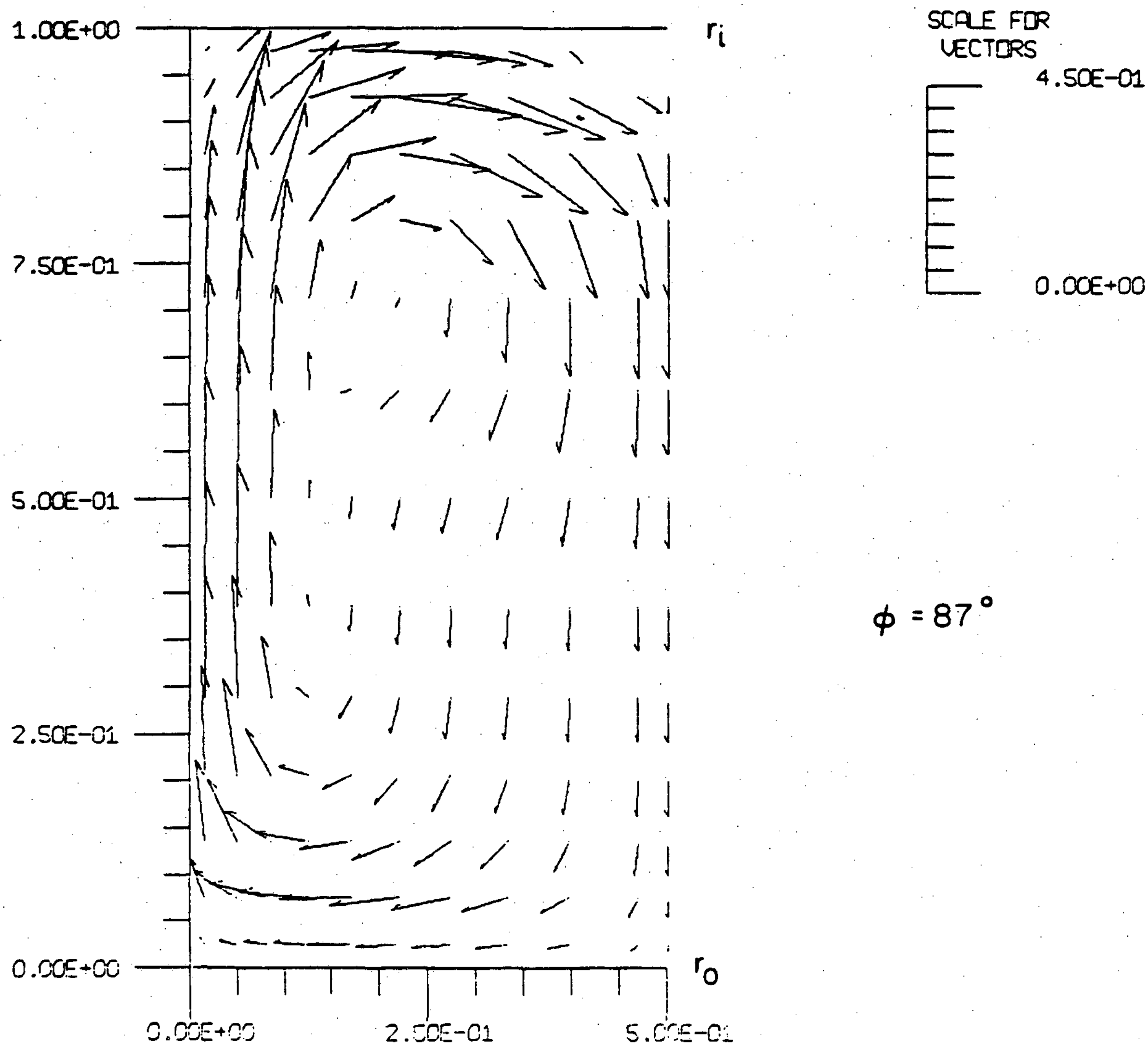

XBL 819-1903

Figure 8 Vector plot of cross-stream velocity components at ϕ = 87 degrees in the curved duct section; case of buoyancy-assisted flow.

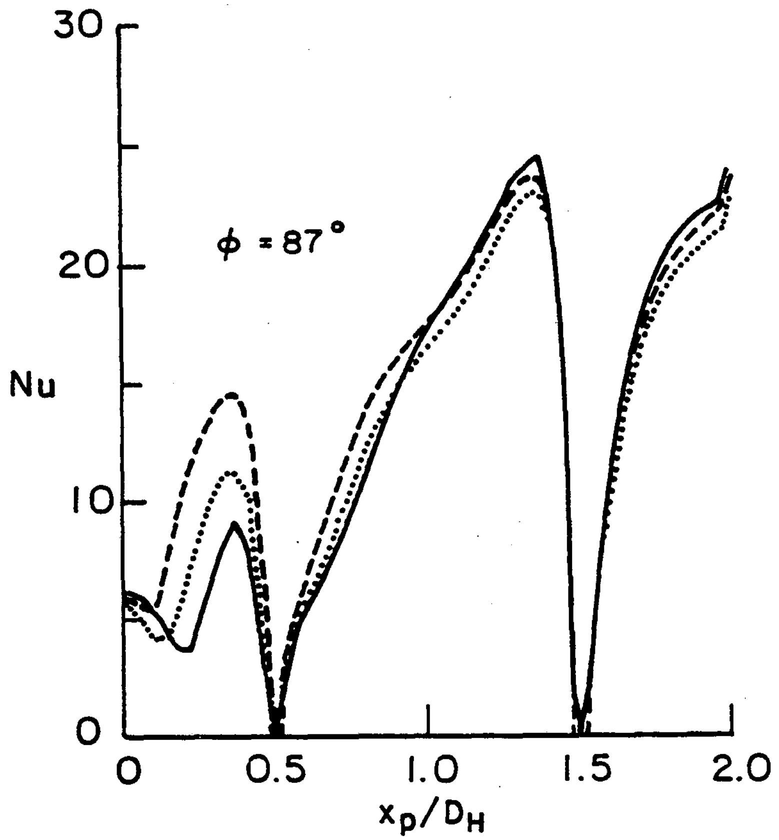

XBL 819-1901

Figure 9 Peripheral variation of local Nusselt number at ϕ = 87 degrees in the curved duct section: (...) non-buoyant flow, (---) buoyancy-assisted flow, (-) buoyancy-opposed flow.

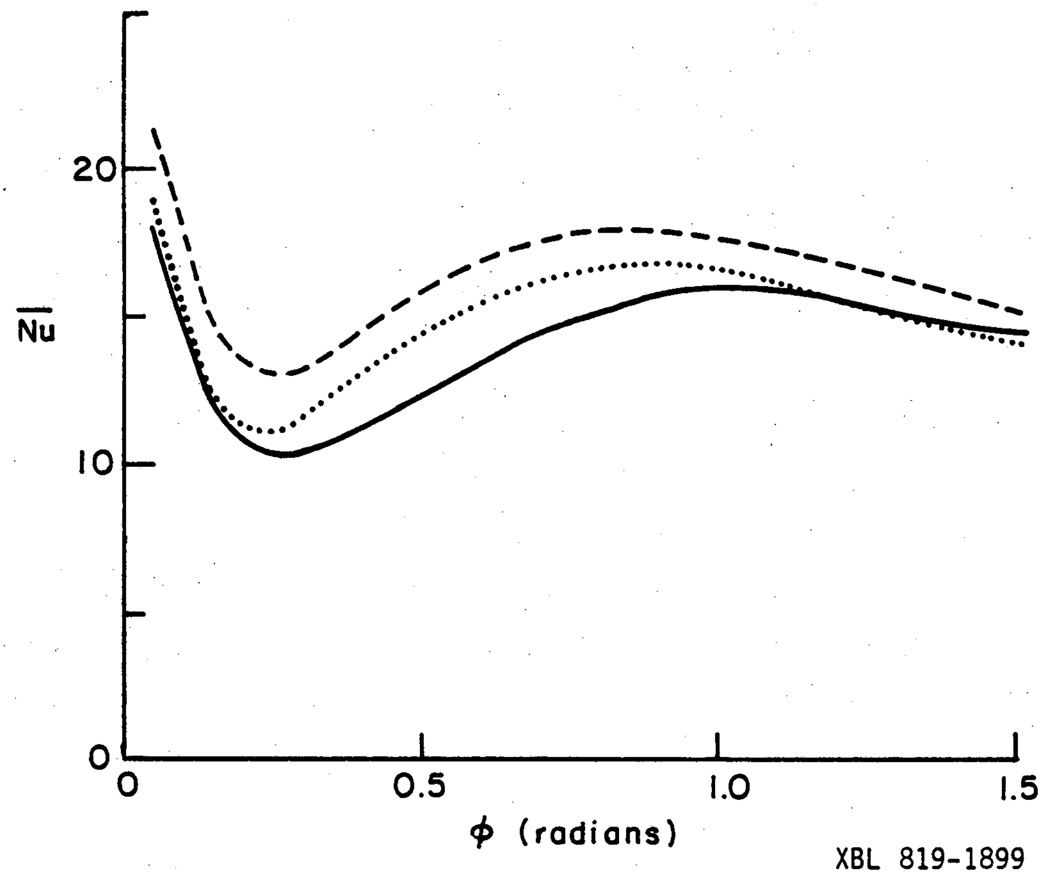

Figure 10 Longitudinal variation of mean Nusselt number in the curved duct section: (...) non-buoyant flow, (---) buoyancy-assisted flow, (-) buoyancy-opposed flow.